Visibility graphlet approach to chaotic time series

Cite as: Chaos **26**, 053107 (2016); https://doi.org/10.1063/1.4951681
Submitted: 22 February 2016 . Accepted: 10 May 2016 . Published Online: 23 May 2016

Stephen Mutua, Changgui Gu and Huijie Yang

Visibility graphlet approach to chaotic time series

Stephen Mutua,[1,2] Changgui Gu,[1,a)] and Huijie Yang[1,a)]
[1]*Business School, University of Shanghai for Science and Technology, Shanghai 200093, People's Republic of China*
[2]*Computer Science Department, Masinde Muliro University of Science and Technology, P.O. Box 190-50100, Kakamega, Kenya*

(Received 22 February 2016; accepted 10 May 2016; published online 23 May 2016)

Many novel methods have been proposed for mapping time series into complex networks. Although some dynamical behaviors can be effectively captured by existing approaches, the preservation and tracking of the temporal behaviors of a chaotic system remains an open problem. In this work, we extended the visibility graphlet approach to investigate both discrete and continuous chaotic time series. We applied visibility graphlets to capture the reconstructed local states, so that each is treated as a node and tracked downstream to create a temporal chain link. Our empirical findings show that the approach accurately captures the dynamical properties of chaotic systems. Networks constructed from periodic dynamic phases all converge to regular networks and to unique network structures for each model in the chaotic zones. Furthermore, our results show that the characterization of chaotic and non-chaotic zones in the Lorenz system corresponds to the maximal Lyapunov exponent, thus providing a simple and straightforward way to analyze chaotic systems. *Published by AIP Publishing.* [http://dx.doi.org/10.1063/1.4951681]

There have been many recent advances in methods for analyzing chaotic time series from the viewpoint of complex networks. Although existing approaches such as recurrence plots and visibility graphs can capture some dynamical behaviors, we must still develop simple and robust methods that can preserve the temporal behaviors of deterministic systems. In this work, we extend the recently proposed visibility graphlet approach to analyze non-trivial behaviors embedded in chaotic time series. Our empirical findings from discrete (Henon and logistic maps) and continuous (Lorenz system) models show that the approach translates the series into a temporal network of networks that entirely preserves both their structural and dynamical behaviors. Furthermore, our results show that the quantitative universality of the period-doubling bifurcation, births of period-3 cycles in the logistic map, intermittency, and the fractal nature of a chaotic series can be visually captured by mapping it into a complex network.

I. INTRODUCTION

Over the past few decades, chaotic motions observed in deterministic systems have attracted interdisciplinary attention because they occur in physical, chemical, biological, ecological, physiological, and social systems.[1] As a result, we must understand chaos to explain various phenomena across numerous domains. Although bifurcation diagrams and other mathematically intense approaches have been extensively used to explain chaos, we must develop simple and robust methods that preserve the dynamic behaviors embedded in a complex system.

One such approach that has gained substantial acceptance across interdisciplinary domains is the use of complex networks.[2–4] Consequently, a number of approaches have been proposed to convert time series into complex networks. Zhang *et al.*[5–7] constructed a complex network from a pseudo periodic time series in which any cycle pairs satisfying a correlation threshold are connected. Xu *et al.*[8–10] proposed linking each node with a predefined number of its closest neighbors. In Refs. 11 and 12, series segments with a predefined length were taken as nodes and linked according to the strength of their correlation. This is a special case of the widely used recurrence networks approach.[13–22] Lacasa *et al.*[23–28] proposed a family of visibility graph algorithms. Each of these approaches was quickly adopted and extensively used to extract information embedded in time series, including chaotic series.[29–32]

However, these approaches do not capture the temporal information of the series. Some interesting concepts have been proposed to monitor dynamics embedded in a time series (e.g., ordinal partition networks) and were summarized in a recent paper by McCullough *et al.*[33] However, more research is required to overcome this problem. The visibility graphlet was recently proposed to mine the dynamical characteristics of a time series.[34] Monitoring the dynamical process of a complex system produces an output series from which one can extract all the series segments with a predefined length. Each of these is taken as representative of the system state corresponding to the specific time interval. The segment is then mapped to a visibility graphlet by linking each pair of elements if they are visible to each other. Linking distinguished graphlets that occur successively leads to a network of visibility graphlets. Detailed works on fractional Brownian motions and stock market observations showed that the visibility graphlet is a powerful approach and can reliably reveal the dynamical behaviors of a complex system.

[a)]Authors to whom correspondence should be addressed. Electronic addresses: gu_changgui@163.com and hjyang@ustc.edu.cn

In this paper, we applied this method to monitor temporal behaviors of deterministic systems that require detailed and systematic tests because they are significantly different from previously investigated stochastic processes. This paper thus seeks to extend and validate the visibility graphlet approach by investigating its ability to preserve the dynamical nature of chaotic series. Most chaotic systems tend to transit from periodic phases to chaotic regimes through period doubling, Feigenbaum scenarios, intermittency transitions, quasi periodicity, and/or crisis approaches.[35] Therefore, we hypothesize that the number of states constructible from such a system should increase significantly in chaotic zones, in a manner similar to the positive Lyapunov exponent. Consequently, various typical points can be easily identified and analyzed in terms of the dynamics of the constructed networks.

Our results indicate that the visibility graphlet approach accurately captures and preserves the evolving temporal features of both discrete (logistic and Henon maps) and continuous (Lorenz flow) chaotic systems. The scaling behaviors of the various typical values show that a chaotic dynamical system exhibits a strong fractal behavior during the chaotic zones. However, whereas the discrete chaotic systems are persistent during the onset to chaos, the continuous system exhibits an anti-persistence that reflects the intermittency, during which the system is neither chaotic nor periodic. Furthermore, the constructed complex networks indicate that all the series convert to regular networks (ring-like structures), similar to the results obtained by McCullough and others[33] when using ordinal partition networks (which retain the temporal information of continuous dynamical systems). Conversely, the periodic zones (islands) between chaotic zones translate to regular networks in discrete maps, but they convert to a random network for the Lorenz system.

II. METHODS AND MATERIALS

A. Chaotic series

We used three classical models to generate the time series data used in this work. These included two discrete maps (Henon and logistic) and a continuous flow model (Lorenz system). To ensure consistency across all the models, each of the series was of length 11 000 and the first 10^3 transient values were truncated (as in a related study by Xu *et al.*[8]). When simulating the Lorenz system, we used a time step of 0.01 s and a sampling rate of 8, implying that the time interval between successive samplings was $0.01\,\text{s} \times 8 = 0.08\,\text{s}$. Accordingly, for window sizes of 6, 7, and 8, the corresponding time intervals were 0.40 s, 0.48 s, and 0.56 s. We also calculated time intervals when using a sampling rate of 1. This was guided by the practical method proposed by Cao,[39] which is extensively used to determine minimum embedding dimensions and time delays for scalar time series. In that paper, the author illustrated the method using a Lorenz system with identical parameter values. It is found that if one uses a sampling rate of 15 and a time step 0.01 s, the minimum embedding dimension is 3. Each vector in the reconstructed phase-space covers a time interval of $0.01\,\text{s} \times 15 \times (3-1) = 0.30$. Hence, the selected parameter values can guarantee that the windows are sufficiently large and reasonable. More detailed formal definitions for each of the models are given in the respective results sections, for ease of reference and coherence.

B. Visibility graphlet analysis

For a given time series, we can extract all the series segments with a predefined length as representatives of the states in the corresponding time durations. We then use the visibility algorithm to further map each representative of a state into an adjacency matrix (graphlet). We now briefly describe this approach but more details can be found in Ref. 34.

Sliding a window of size w along time series $Y = \{y_1, y_2, \ldots, y_N\}$ results in $Y_k = \{y_k, y_{k+1}, \ldots, y_{k+w-1}\}$, where $k =, 1, 2, \ldots, N-w+1$. Given two values y_i and y_j $(i<j)$, the two elements are visible if all the values between them (i.e., y_k $(i<k<j)$) satisfy

$$y_k \leq y_i + (y_j - y_i)\cdot\frac{j-k}{j-i}. \tag{1}$$

In each resulting segment Y_k, if any pair of elements are visible, they are linked by an edge.[23] The generated visibility graphlets contain vital structural features and fully describe the states of the complex system over time.

The visibility graphlet corresponding to the k'th segment can be represented by an adjacency matrix, g_k, where the element $g_k(a-k+1, b-k+1)$ equals 1(0) if the corresponding pair of elements (y_a and y_b) in the segment are visible (invisible). Here, the identification numbers of the nodes corresponding to y_a and y_b are set to $a-k+1$ and $b-k+1$, to ensure that they are in the interval $[1, w]$, resulting in a w by w matrix. Covering the whole series, we obtain a set of adjacency matrices, $G = \{g_1, g_2, \ldots, g_{N-w+1}\}$.

Consequently, we define a state transfer network to describe the transfer probabilities between distinguishable states. In the time series, if a state at time b occurs immediately after another state at time a, a directional link is constructed from g_a to g_b. The link represents a transfer from one state to the other state, resulting in a state chain with directional links as indicated by

$$g_1 \rightarrow g_2 \rightarrow \cdots \rightarrow g_{N-w+1}. \tag{2}$$

We scan through G comparing each state with the others. If any two states are identical (their adjacency matrices are the same), we replace the later one with the reference state. For instance, if $g_1 = g_6$, the state g_6 is replaced with g_1. This procedure is applied iteratively for all states. The survivors are unique states, which are defined as nodes. By determining the number of links between each pair of the nodes (survival states), we can obtain the weight of the link between them. Consequently, the time series is mapped to a directed and weighted "network of networks" of distinguishable states (state transfer network), so that all possible network established computations can be performed on demand. The steps of the visibility graphlet algorithm are summarized and illustrated in Fig. 1.

However, the key challenge is selecting the appropriate window size for the phase space reconstruction. Reference 34 contains a detailed discussion of this problem. For a

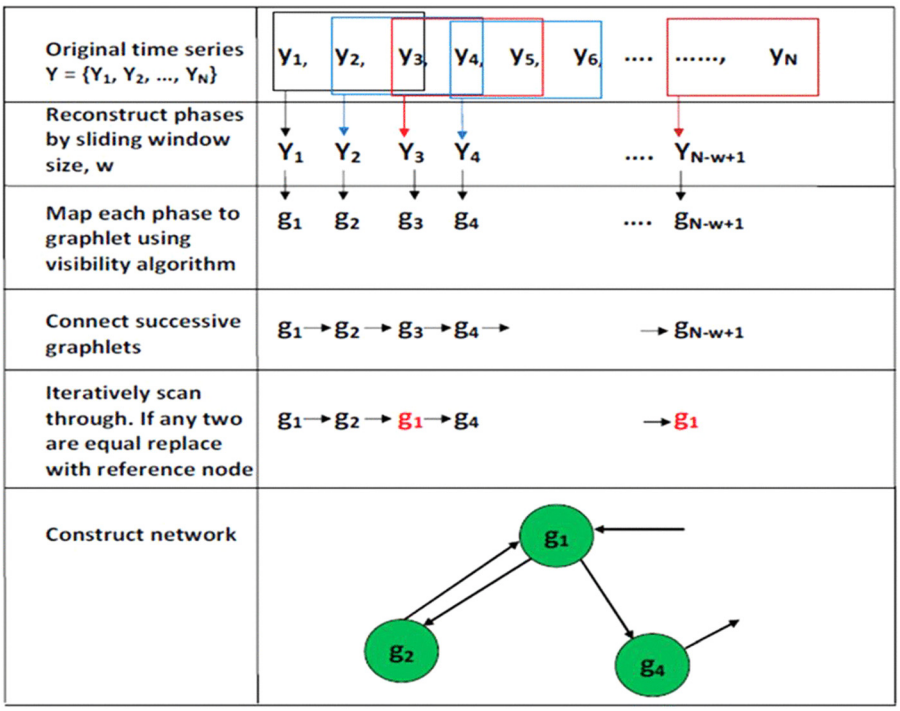

FIG. 1. Constructing a network from an initial time series after normalization, using the visibility graphlet approach. The window size (w = 3) is used for illustration purposes only.

chaotic process, the window size can be simply selected to be equal to or larger than the embedded dimension of the time series in the phase space reconstruction framework. Linking successive distinguished graphlets provides a natural way to track a dynamic process. This successive occurrence is physically much more meaningful than an artificially defined proximity based on a mathematically calculated distance.

III. RESULTS AND DISCUSSION

A. Preserving dynamic properties

1. Henon map

The Henon map is a discrete dissipative system that was proposed by Henon[36] and is formally defined as

$$\begin{aligned} x_{n+1} &= 1 - \alpha x_n^2 + y_n, \\ y_{n+1} &= \beta x_n. \end{aligned} \tag{3}$$

The map depends on two parameters, α and β. In the classical map, $\alpha = 1.4$ and $\beta = 0.3$ represent a chaotic system. For other parameter values, the model may be chaotic, intermittent, or periodic. Using α as the control parameter, we studied the behavior of the map using the graphlet approach. Figure 2 presents our results when using the initial values $x_0 = y_0 = 0.5$.

Figure 2 shows various interesting zones marked with letters (a–h), during which various system dynamics occurred. Each of these sections is mapped into a Henon map (corresponding to the section letter) shown on the right of Fig. 2.

The map is stable for values $1.01 \leq \alpha \leq 1.09$ ((a) and (b) of Fig. 2) when the system is periodic. When $\alpha \leq 1.1$, the period doubles, increasing the number of states and leading to the onset of chaos. The period doubling occurs at an increased rate, and there is a continuous increase in the number of states ((c) of Fig. 2). At $\alpha \approx 1.15$, the system becomes chaotic, which persists until $\alpha = 1.22$ (d) when the system enters a lengthy periodic window between $1.23 \leq \alpha \leq 1.27$ ((e) in Fig. 2). This periodic state tends to occur for most initial values of x and y, before the system returns to the chaotic zone (f) and slows to $\alpha = 1.3$ (g), dependent on the initial condition. Some initial conditions may result in a total periodic window at $\alpha = 1.3$, but others do not and perturbations are observable. The system remains chaotic ((h) in Fig. 2) and then the values rapidly increase to infinity for all values of $\alpha \geq 1.44$.

2. Lorenz system

First proposed by Edward Lorenz to explain the convection in the earth's atmosphere,[37] the Lorenz system is a set of three ordinary differential equations defined as

$$\begin{aligned} \frac{dx}{dt} &= \sigma(y - x), \\ \frac{dy}{dt} &= x(\rho - z) - y, \\ \frac{dz}{dt} &= xy - \beta z. \end{aligned} \tag{4}$$

Here, x, y, and z define the system state; t is the time; and σ, ρ, and β are the system parameters. Lorenz proposed and used the classical parameter values $\sigma = 10$, $\rho = 28$, and $\beta = 8/3$, during which the system is in chaos. We used the adaptive 4th and 5th order Runge-Kutta method to solve the differential equations[38] and used ρ as the control parameter (which varied between 13 and 150).

Figure 3 shows the dynamical properties of the model when using various window sizes for different typical points (shown in the subplots labeled (a–f)). For the early values $13 \leq \rho \leq 17$, the system is stable between two fixed points but the periodicity increases with ρ. For instance, at values

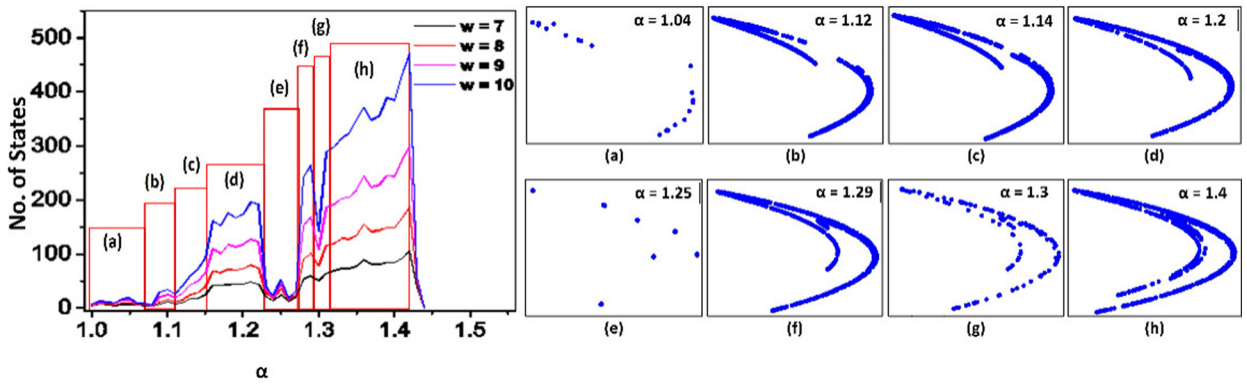

FIG. 2. Preserving the structure of a Henon map. In (i), the left graph is subdivided to reflect changes when applying the graphlet approach. On the right, the map's significant changes (as observed in the bifurcation diagram) are matched to corresponding parts of the left side. In (ii), typical values are selected from each of the subdivisions, and an orbit diagram shows the corresponding evolutionary behavior.

$17 < \rho \leq 20$, the number of nodes increases significantly compared with the previous stable values, and a strange attractor is briefly observed. At $\rho = 19$, intermittent chaos (characterized by a sudden increase of states in Fig. 3) is observed before returning to a stable state within $20 < \rho \leq 23$ (see Fig. 3 for the decreased states). The system enters a chaotic state for values beyond $\rho = 24$, typified by a constant high number of states. This continues with increasing values of ρ, except for $92 \leq \rho \leq 93, 99 < \rho \leq 101, 132 < \rho \leq 133$, and $\rho > 146$, during which the system experiences periodic windows characterized by sudden decreases in the number of states irrespective of the window size.

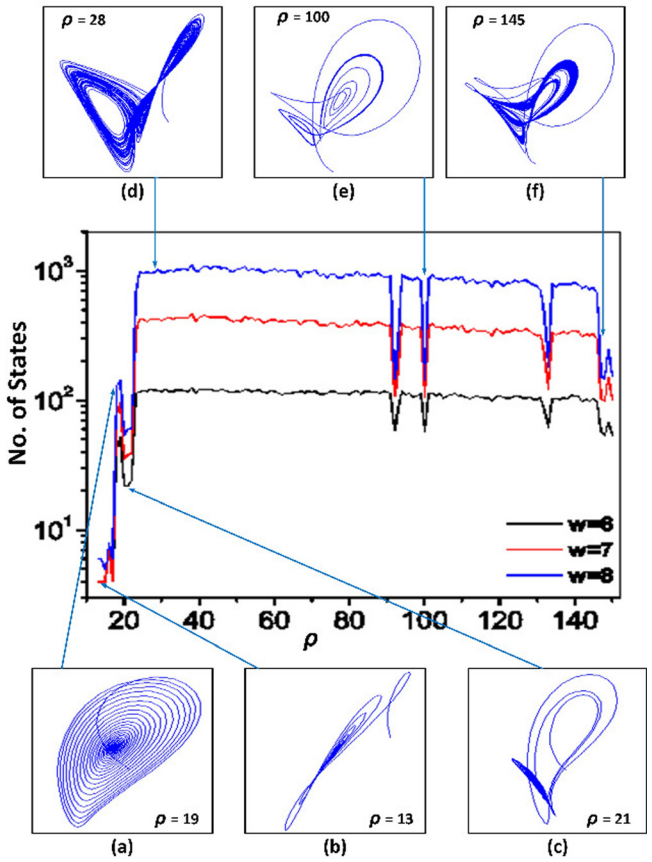

FIG. 3. Preserving the dynamic properties of Lorenz's system. Various dynamic states are represented by various numbers of constructible states using window sizes of 6, 7, and 8, and a sampling rate of 1. The marked sections show that the system properties are preserved regardless of the window size, as shown for the initial stages of the system (a, b), onset to chaos (c), chaotic zones (d), and "islands" between the chaotic zones (e, f).

Lyapunov exponents are commonly used to determine the state of a deterministic system, in which a positive exponent indicates chaos. Figure 4 compares the results obtained using the visibility graphlet approach and the largest Lyapunov exponent calculated according to Ref. 40. Figure 4(a) shows that the number of constructible states depends on the state of the system, a phenomenon observed in Fig. 4(b) when using the largest Lyapunov exponents. Furthermore, to ensure the system is independent of the window size, we ran the system with window sizes 6, 7, and 8 and a sampling rate of 8. Figure 4(c) shows the results and indicates that there is a similar trend to Fig. 4(a) (in which the sampling rate was 1) and Fig. 4(b) (the maximal Lyapunov exponents method). Although there are a reduced number of states for each window size, it is notable that the approach produces accurate results that agree with the system dynamics despite the delay and embedding dimension parameters. The proposed approach thus reliably retains the system dynamics of a chaotic series and can be used as a tool for mining modeled chaotic data and real data with a chaotic nature.

3. Logistic map

The logistic map was first proposed by May[41] to predict insect populations at time $t + \Delta t$. Many researchers have studied its complicated dynamics and universality. Formally, the logistic equation is

$$x_{t+1} = r x_t (1 - x_t). \tag{5}$$

We investigated the node frequency of the model using the initial value $x_0 = 0.4$, letting r vary between 0 and 4.

For $0 < r < 1$, $n \to \infty$, and any $x_0 \in [0, 1]$, the system settles to a single fixed point that is characterized by a single node when using the visibility graphlet approach (Fig. 5). For $1 < r < 3$, the system settles to two fixed values. This phenomenon corresponds to only two states in the visibility graphlet approach. For $r = 3$, first, pitchfork bifurcations occur and develop into similar individual occurrences throughout the system, and the period-two cycles are

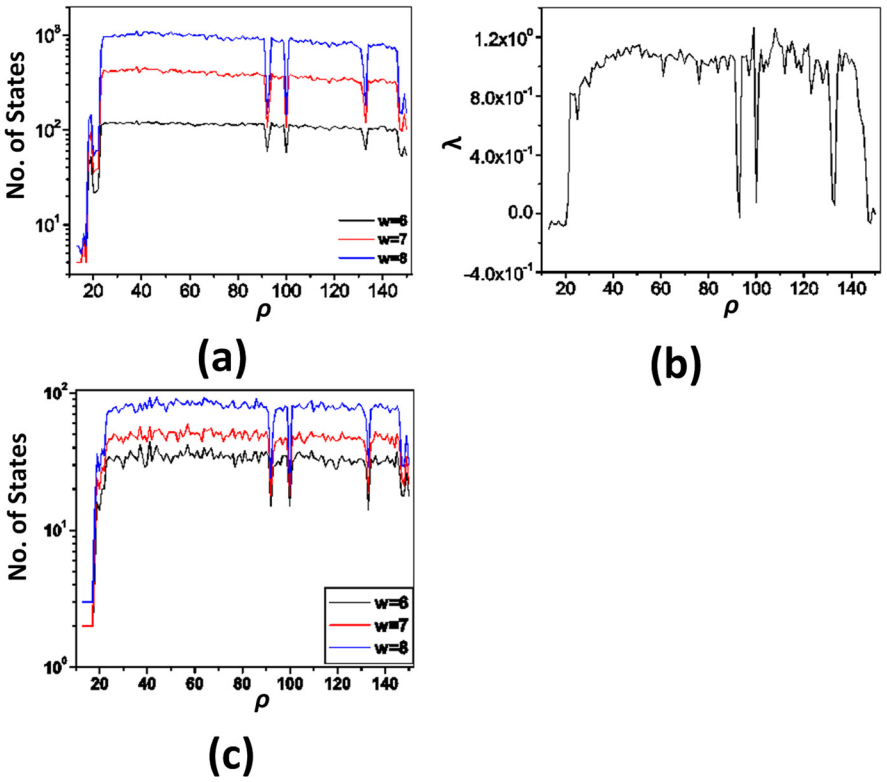

FIG. 4. Comparing the frequency of states realized using the visibility graphlet approach and the maximum Lyapunov exponent. In (a), various window sizes sampled at time steps of 0.01 s and a rate of 1 show sudden decreases in the significant points. This is similar to (b), which corresponds to the maximal Lyapunov exponents and is positive during chaotic states and negative for various periodic windows of the Lorenz system. A sample rate of 8 (as indicated in (c)) produced qualitatively similar results to (a) and (b).

replaced with higher period cycles. The graphlet approach accurately captures this onset of the quantitative universality of the period-doubling bifurcation using an increase in the number of states. This is shown in Fig. 5 and continues to

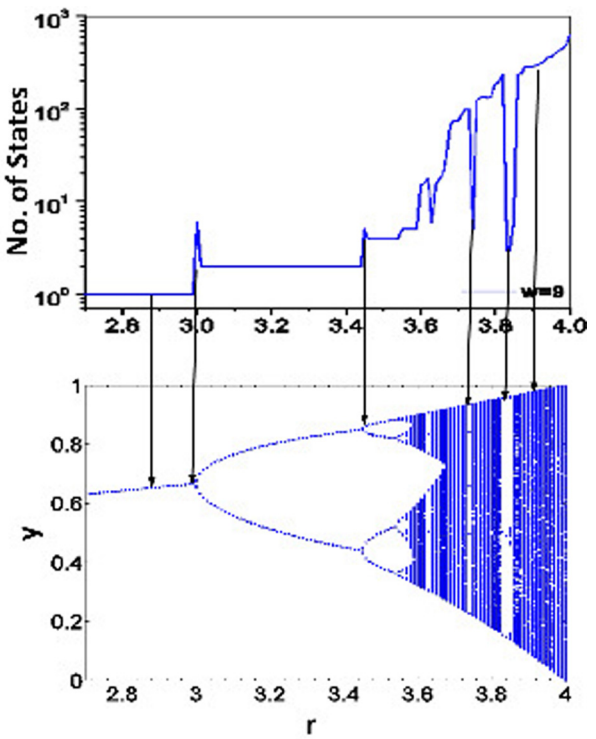

FIG. 5. Preserving the dynamic properties of the logistic system. Compares the structural properties of the logistic model with respect to a bifurcation diagram on the left with the results from the graphlet visibility approach using a sliding window size of w = 9. The arrows mark critical values where the system assumes different states. $r = 3$ and $r = 3.45$ correspond to period doubling and $r = 3.74$ and $3.82 \leq r \leq 3.84$ are periodic windows between chaotic zones.

$r < 1 + \sqrt{6} \approx 3.449$. Faster period doublings continue, before the system converges to a critical point $r_c \approx 3.56$, during which the system is chaotic for most values of $r > r_c$. This phenomenon corresponds to a high number of constructible states in Fig. 5.

However, islands of stability are observed at $r = 3.74$ and $3.82 \leq r \leq 3.84$, as illustrated in the bifurcation diagram to the right of Fig. 5 and the plot on the left (graphlet approach). The last stable period is the longest, which is a prominent 3-cycle window that occurs via a tangent bifurcation at $r = 1 + \sqrt{8}$. This marks the start of higher period cycles and corresponds with a sudden decrease in the number of states in the graphlet approach. These results agree with various other studies.[42–45]

B. Network structural properties

In this section, we explore the various global and local properties of the three chaotic model networks. We analyzed the topological properties of each network to see if they can be used to differentiate the dynamics of the systems. Furthermore, we evaluated how well the overall system dynamics captured the temporal behaviors of the series by exploring the scaling properties of their motifs.

1. Topological properties

The frequency that a node occurs is called its *degree*. The proposed method results in a directed weighted network, so each node has an in-degree, out-degree, and weighted degree. The weighted degree is also referred to as the node strength and is the sum of weights attached to the ties that belong to a node.[46] A hub node has a significantly larger degree than the other nodes. Hubs are easily determined, but they may be common in even randomly shuffled models and

TABLE I. Summary of various topological structural properties of the constructed networks of the three models for three typical values during which the system exhibits period doubling (bifurcation), the onset of chaos, chaos, or occasional periodic windows (the window size is w = 6).

Model	Parameter	Model status	Nodes frequency	Diameter	Av. weighted degree $\langle w \rangle$	Av. path length $\langle l \rangle$
Lorenz	$\rho = 14$	Homoclinic bifurcation	4	3	2498.25	2
	$\rho = 21$	Onset to chaos	22	10	464.44	5.09
	$\rho = 25$	Chaos	119	8	83.98	4.10
	$\rho = 100$	Aperiodic window	58	12	172.29	5.278
Logistic	$r = 3.45$	Periodic doubling	4	3	2498.25	2
	$r = 3.6$	Onset to chaos	7	4	1284.571	2.381
	$r = 3.99$	Chaos	48	8	187.354	4.097
	$r = 3.84$	Periodic window	3	2	2997.67	1.5
Henon	$\alpha = 1$	Periodic doubling	4	3	2498.25	2
	$\alpha = 1.14$	Onset to chaos	11	8	817.545	3.4
	$\alpha = 1.42$	Chaos	54	10	166.537	4.688
	$\alpha = 1.24$	Periodic window	7	6	1284.714	3.5

thus have less non-trivial characteristics. If a node's degree in the original time series is significantly larger than that in a shuffled time series, the node is called a motif[47,48] and can be used as a global representation of the system.

The *diameter* of a network is the shortest distance between the two most distant nodes in the network. It is simply the longest of all the calculated path lengths. It is a measure of the density of a network. A disconnected network has an infinite diameter.

Using these global network properties, we studied the three chaotic models to see if, when combined with the average path length, they can appropriately distinguish between the various zones of a dynamic system. Table I contains a summary of four typical points for each model, which correspond to a bifurcation, the onset of chaos, a chaotic zone, and a periodic window.

It is clear that the structural properties are not sufficient to distinguish between various states of a chaotic series. The average weighted degree varies appropriately and perhaps would be the best metric in this case. However, it is directly proportional to the number of nodes. Therefore, we should not needlessly implement additional computations for something that is readily observable. Further, the visual characteristics of the networks present a rather interesting scenario, as shown in Fig. 6. When all the models reach a period doubling stage, the constructed networks are regular and have ring structures (Figs. 6(a1), 6(b1), and 6(c1)). Thus, there is a clustering coefficient of 0. During chaotic states, the networks are characterized by the existence of hubs and several low degree nodes, as seen in Figs. 6(a4), 6(b4), and 6(c4). Similarly, the discrete maps (Henon and logistic) converge to a regular ring network during

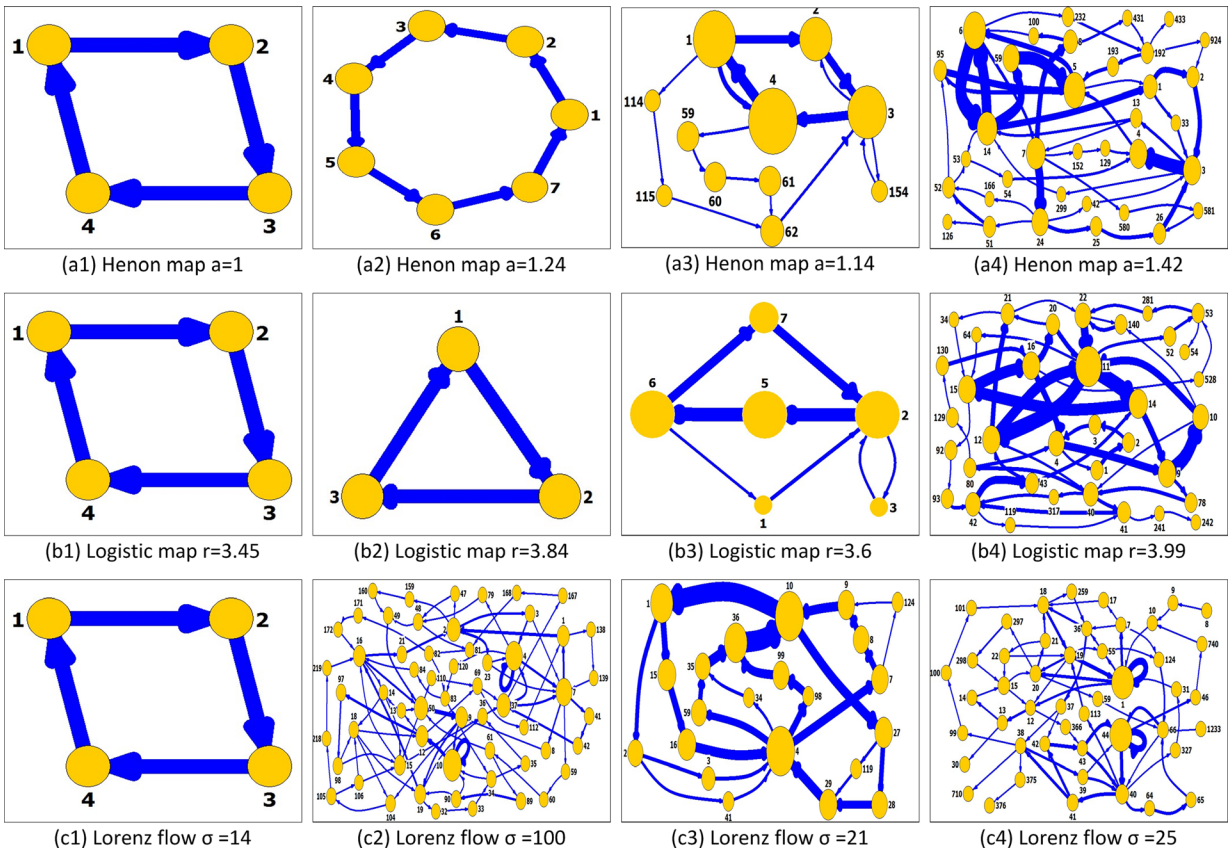

FIG. 6. State transfer networks of chaos models for a window size of w = 6, where weak links with weights less than 50 were removed. The networks in (a1), (b1), and (c1) have network structures similar to the periodic states of the Henon, logistic, and Lorenz systems, respectively. (a2), (b2), and (c2) show the models for typical values during which periodic windows occur between chaotic zones. (a3), (b3), and (c3) show the onset of chaos, and (a4), (b4), and (c4) show the states in chaotic zones.

the periodic cycles, as shown in Figs. 6(a2) and 6(b2). However, the Lorenz model results in a network that is similar to the chaotic state, with hubs exhibiting strong self-loops (Fig. 6(c2)). Additionally, although the constructed networks vary globally when using different sampling rates, qualitatively the temporal behaviors have similar characteristics. When the sampling rate was 8, the constructed networks for periodic and chaotic zones all converged to a simple star topology. However, when the period doubled, a ring structure was again observed. The star networks are also characterized by hubs that exhibit strong self-loops, especially in the chaotic zones. During the onset to chaos, all the models present unique properties characterized by a transition from period doubling into chaos. For instance, both maps have strong similarities to period doubling networks, as seen in the nodes of closed cycles (e.g., $1 \rightarrow 2 \rightarrow 3 \rightarrow 4 \rightarrow 1$ in Fig. 6(a3) and $2 \rightarrow 5 \rightarrow 6 \rightarrow 7 \rightarrow 2$ in Fig. 6(b3)). However, the Lorenz model indicates an increase in states, because two main hubs (nodes 4 and 10) appear and seem to control the network in Fig. 6(c3).

2. Scaling properties

Each of these constructed nodes is a culmination of the diffusion trajectory of unique subgraphs (visibility graphlets) along the time series. They retain the local connectivity and behaviors of the system at any given point and thus represent the temporality within the series. A natural question that arises is whether these temporally occurring series retain the universally known characteristics of chaotic series. To address this, we computed and analyzed the scaling properties of typical values within the series to test for the long-term memory that is expected with chaotic series.

Many researchers have reported self-similar structures in time series from diverse applications (see, e.g., Ref. 49). Chaotic series are characterized by fractality and universality, so we studied the scaling properties of motifs from the various states of the three models. As previously mentioned, although hubs are easily observed, their existence may be ordinary and equally observable in null models. However, if a given state occurs much more frequently in the original time series than in the shuffled time series, the state represents a special global feature of the series and is referred to as a *motif*.

We investigated the scaling behavior of the motifs using re-scaled range analysis (R/S).[50] We can record the positions of a specified motif and denote them by $\omega_k, k = 1, 2, \ldots, M$, where M is the frequency at which the motif occurs. The incremental series is $\omega_{k+1} - \omega_k, k = 1, 2, \ldots, M-1$. All possible segments with length n are $\Omega^j \equiv (\omega_{j+1} - \omega_j,\ \omega_{j+2} - \omega_{j+1}, \ldots, \omega_{j+n} - \omega_{j+n-1}), j = 1, 2, \ldots, M-n$. The corresponding accumulated departures for the jth segment can be constructed using

$$\Phi^j(i) \equiv \sum_{w=1}^{i} [\Omega^j(w) - \langle \Omega^j \rangle] = \omega_{j+i} - \omega_j - \frac{i}{n}(\omega_{j+n} - \omega_j), \quad i = 1, 2, \ldots, n. \tag{6}$$

The re-scaled range is estimated using

$$R/S(n) \equiv \langle R^j/S^j(n) \rangle = \frac{1}{M-n} \sum_{j=1}^{M-n} \frac{max\left[\Phi^j(1), \Phi^j(2), \ldots, \Phi^j(n)\right] - min\left[\Phi^j(1), \Phi^j(2), \ldots, \Phi^j(n)\right]}{std(\Omega^j)}. \tag{7}$$

If there exists scale invariance in these positions, we have $R/S(n) \sim n^{\delta}$, where δ is the Hurst exponent. The results are presented in Fig. 6 for different states of the three chaotic models, that is, onset to chaos, chaos, and Lorenz's aperiodic window.

The models have periodic cycles during the initial stages of the systems. They all converge to two fixed points characterized by cyclic regular networks (see Figs. 6(a1), 6(b1), and 6(c1)) in which the systems are highly predictable. The Henon and logistic maps converge to periodic zones of different cycles, illustrated by different regular networks. The Henon settles to an increased number of states (from 4 to 7), as shown in Fig. 6(a2), but the logistic has a lower number of states (3) that all occur deterministically, as shown in Fig. 6(b2). However, the Lorenz system has a unique characteristic that it is neither chaotic nor periodic. Figure 6(c2) shows that the network has two main highly attractive hubs and several equal degree nodes. Furthermore, the identified motifs are very random with unpredictable scalability, as shown in Figs. 7(d1) and 7(d2). This corresponds to the intermittency of the Lorenz system, which behaves almost periodically for some time and then behaves chaotically before returning to the periodic state. This continues infinitely and randomly and is seen in Fig. 7(d1) for motifs 1 and 2, and Fig. 7(d2) for motifs 3 and 4.

At the onset to chaos, Henon motifs are fractal with Hurst exponents of 0.57, 0.55, 0.58, and 0.57 for motifs 1 to 4, respectively, as shown in Fig. 7(a1). The same phenomenon is observed in the logistic map with exponents of 0.64, 0.63, 0.58, and 0.63 for the four motifs, as shown in Fig. 7(b1). However, the Lorenz system is anti-persistent and almost random, as observed in Fig. 7(c1). These motifs have Hurst exponents of 0.44, 0.46, 0.4, and 0.37 for motifs 1 to 4, respectively. Chaos is characterized by fractality and universality. This can be seen in the scaling behavior of the three models (Figs. 7(a2) to 7(c2)), which have various persistent motifs. The Henon map has motifs with exponents of 0.6, 0.71, 0.57, and 0.54 (Fig. 7(a2)), the logistic map has motifs with exponents of 0.73, 0.57, 0.45, and 0.75 (Fig. 7(b2)), and the Lorenz system has motifs with exponents of 0.69, 0.63, 0.55, and 0.63 (Fig. 7(c2)). From these results, it is evident that the visibility graphlet approach completely preserves the

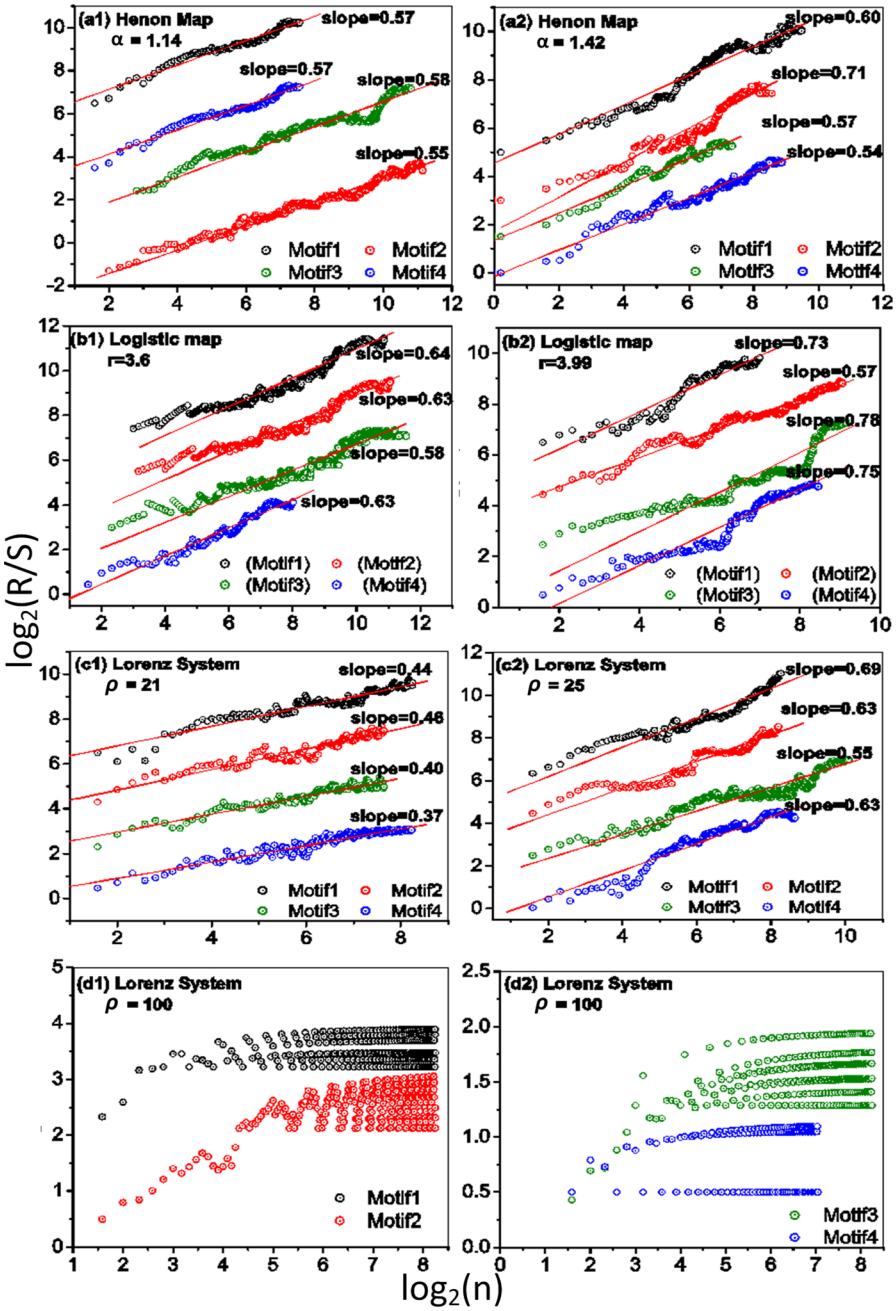

FIG. 7. Persistent behaviors of the motifs for the Henon, logistic, and Lorenz systems for various states and a window size of w = 6. (a1), (b1), and (c1) show the three models at the onset of chaos; (a2), (b2), and (c2) correspond to the chaotic state, and (d1) and (d2) demonstrate the randomness during the periodic window of the Lorenz System, which is neither chaotic nor periodic.

structural and internal properties of a chaotic series. Although the number of constructible states is comparable to a bifurcation diagram and the largest Lyapunov exponent, the obtained scaling properties are representative of the internal structure of the system.

IV. CONCLUSION

We used the visibility graphlet approach to show that various structural and dynamical features of discrete and continuous chaotic models can be preserved using complex networks. The well-known properties of the logistic map were clearly expressed, including pitchfork bifurcations, period doublings, the onset of chaos, and chaos. For $r = 3$, the initial bifurcations occurred and moved from fixed point attractors to 2^k cycles, which increase with r. As expected, periodic islands occurred between chaotic states. The longest was observed during [3.82, 3.84], when period-3 cycles began. Chaos was characterized by a strong fractal nature demonstrated by a motif with a maximum Hurst exponent of 0.75.

The 2D Henon map is characterized by a period doubling route to chaos, similar to the logistic map. It experienced a lengthy periodic window for $1.23 \leq \alpha \leq 1.27$, during which the system was periodic and had a cyclic regular network with a clustering coefficient of zero. However, at $\alpha \approx 1.3$, the system was intermittent, characterized by incomplete chaos (corresponding to the Lorenz model with $\rho \approx 100$). Similarly, chaos was very persistent when the leading Hurst exponent was 0.71.

The dynamic characteristics of the Lorenz system are typified by a varying number of constructed nodes, similar to discrete models. Although the system remained stable before the initial homoclinic bifurcation at $\rho \approx 14$, it became

periodic for $13 < \rho \leq 17$. However, an increase in ρ caused a significant increase in the number of attractors, and at $\rho > 24$, the system became chaotic (characterized by a sudden increase in the number of network nodes). We can observe this state in the scaling behaviors of the motifs that have Hurst exponents that satisfy $H > 0.5$. Nonetheless, periodic windows were observed at values such as $\rho \approx 92$ and $99 < \rho < 101$. In the latter case, the system was intermittent before it returned to a chaotic state. Other similar windows occurred during $132 < \rho < 134$ and $\rho > 146$, which were also observed in Ref. 51.

These results were observed when using sampling rates of 8 and 1 and qualitatively follow the same trend as a plot of the maximal Lyapunov exponents. This corresponds to the various numbers of constructible states when using the visibility graphlet, similar to results obtained using ordinal partitions.[33] A positive exponent corresponds to regions that have a large number of constructible states, and a negative exponent corresponds to sudden decreases. However, the continuous nature of the network means that different sampling rates may result in structurally different complex networks and various global network metrics. Nevertheless, the qualitative temporal features of the system are retained and the constructible states serve as an indicator of the system dynamics, regardless of the parameters.

In summary, we proposed a graphlet approach that can be used to understand chaotic time series. We extended earlier work[34] and showed that the approach can accurately preserve the dynamic and topological features of chaotic series. This provides a method for constructing complex networks from chaotic time series and supplements the commonly used Lyapunov exponent when detecting the presence of chaos. Therefore, we can construct complex networks without imposing an artificial threshold using visibility graphlets to capture the local states and identify their occurrences.

ACKNOWLEDGMENTS

The work was supported by the National Natural Science Foundation of China under Grant Nos. 10975099 and 11505114, the Program for Professor of Special Appointment (Orientational Scholar) at Shanghai Institutions of Higher Learning under Grant Nos. D-USST02 (H. Yang) and QD2015016 (C. Gu), the Shanghai project for construction of discipline peaks under Grant No. USST-02-SAI, and the Innovation Program of Shanghai Municipal Education Commission under Grant No. 13YZ072. We thank the reviewers for their stimulating and constructive comments and suggestions.

[1]S. Vinita, P. Awadhesh, and S P. Harinder, "Nonlinear time series analysis of sunspot data," Sol. Phys. **260**(2), 441–449 (2009).
[2]D. J. Watts and S. H. Strogatz, "Collective dynamics of 'small-world' networks," Nature **393**, 440–442 (1998).
[3]A. Barabasi and A. Reka, "Emergence of scaling in random networks," Science **286**(5439), 509–512 (1999).
[4]S. H. Strogatz, "Exploring complex networks," Nature **410**, 268–276 (2001).
[5]J. Zhang and M. Small, "Complex network from pseudoperiodic time series: Topology versus dynamics," Phys. Rev. Lett. **96**, 238701 (2006).
[6]J. Zhang, X. Luo, T. Nakamura, J. Sun, and M. Small, "Detecting temporal and spatial correlations in pseudoperiodic time series," Phys. Rev. E **75**, 016218 (2007).
[7]J. Zhang, J. Sun, X. Luo, K. Zhang, T. Nakamura, and M. Small, "Characterizing pseudoperiodic time series through the complex network approach," Physica D **237**, 2856–2865 (2008).
[8]X. Xu, J. Zhang, and M. Small, "Superfamily phenomena and motifs of networks induced from time series," Proc. Natl. Acad. Sci. U.S.A. **105**(50), 19601–19605 (2008).
[9]J. Zhang, C. Zhou, X. Xu, and M. Small, "Mapping from structure to dynamics: A unified view of dynamical processes," Phys. Rev. E **82**, 026116 (2010).
[10]R. Xiang, J. Zhang, X. Xu, and M. Small, "Multiscale characterization of recurrence-based phase space networks," Chaos **22**, 013107 (2012).
[11]Y. Yang and H.-J. Yang, "Complex network-based time series analysis," Physica A **387**, 1381–1386 (2008).
[12]Z. Gao and N.-D. Jin, "Flow-pattern identification and nonlinear dynamics of gas-liquid two-phase flow in complex networks," Phys. Rev. E **79**, 066303 (2009).
[13]N. Marwan, J. F. Donges, Y. Zou, R. V. Donner, and J. Kurths, "Complex network approach for recurrence analysis of time series," Phys. Lett. A **373**, 4246–4254 (2009).
[14]R. Donner, Y. Zou, J. Donges, N. Marwan, and J. Kurths, "Recurrence networks—A novel paradigm for nonlinear time series analysis," New J. Phys. **12**(3), 033025 (2010).
[15]R. Donner, Y. Zou, J. Donges, N. Marwan, and J. Kurths, "Ambiguities in recurrence based complex network representations of time series," Phys. Rev. E **81**, 015101(R) (2010).
[16]R. Donner, M. Small, J. Donges, N. Marwan, Y. Zou, R. Xiang, and J. Kurths, "Recurrence-based time series analysis by means of complex network methods," Int. J. Bifurcation Chaos **21**, 1019–1046 (2011).
[17]Y. Zou, J. Heitzig, R. Donner, J. Donges, J. Farmer, R. Meucc, S. Euzzor, N. Marwan, and J. Kurths, "Power-laws in recurrence networks from dynamical systems," Europhys. Lett. **98**, 48001 (2012).
[18]Z. Gao, X. Zhang, M. Du, and N. Jin, "Recurrence network analysis of experimental signals from bubbly oil-in-water flows," Phys. Lett. A **377**, 457–462 (2013).
[19]Z. Gao, X. Zhang, N. Jin, R V. Donner, N. Marwan, and J. Kurths, "Recurrence networks from multivariate signals for uncovering dynamic transitions of horizontal oil-water stratified flows," Europhys. Lett. **103**, 50004 (2013).
[20]Z. Gao, X. Zhang, N. Jin, N. Marwan, and J. Kurths, "Multivariate recurrence network analysis for characterizing horizontal oil-water two-phase flow," Phys. Rev. E **88**(3), 032910 (2013).
[21]D. Eroglu, T. Peron, N. Marwan, F. Rodrigues, L. Costa, M. Sebek, I. Kiss, and J. Kurths, "Entropy of weighted recurrence plots," Phys. Rev. E **90**, 042919 (2014).
[22]Y. Zou, R. Donner, and J. Kurths, "Analyzing long-term correlated stochastic processes by means of recurrence networks: Potentials and pitfalls," Phys. Rev. E **91**, 022926 (2015); Z.-K. Gao, P.-C. Fang, M. S. Ding, D. Yang, and N.-D. Jin, Complex networks from experimental horizontal oil-inwater flows: Community structure detection versus flow pattern discrimination, Phys. Lett. A **379**, 790–797 (2015); *Recurrence Quantification Analysis: Theory and Best Practices*, edited by C. L. Webber, Jr. and N. Marwan (Springer, 2015), pp. 101–163.
[23]L. Lacasa, B. Luque, F. Ballesteros, J. Luque, and C. Nuno, "From time series to complex networks," Proc. Natl. Acad. Sci. U.S.A. **105**(13), 4972–4975 (2008).
[24]B. Luque, L. Lacasa, F. Ballesteros, and J. Luque, "Horizontal visibility graphs: Exact results for random time series," Phys. Rev. E **80**, 046103 (2009).
[25]L. Lacasa, A. M. Nunez, E. Roldan, J. M. R. Parrondo, and B. Luque, "Time series irreversibility: A visibility graph approach," Eur. Phys. J. B **85**, 217 (2012).
[26]A. M. Nunez, B. Luque, L. Lacasa, and J. P. Gomez, "Horizontal visibility graphs generated by type-I intermittency," Phys. Rev. E **87**, 052801 (2013).
[27]A. M. Nunez, L. Lacasa, and J. P. Gomez, "Horizontal Visibility graphs generated by type-II intermittency," J. Phys. A **47**, 035102 (2014).
[28]L. Lacasa, "On the degree distribution of horizontal visibility graphs associated with Markov processes and dynamical systems: Diagrammatic and variational approaches," Nonlinearity **27**, 2063–2093 (2014).
[29]B. Luque, L. Lacasa, F. J. Ballesteros, and A. Robledo, "Feigenbaum Graphs: A complex network perspective of chaos," PLoS One **6**, e22411 (2011).

[30]L. Lacasa and T. Raul, "Description of stochastic and chaotic series using visibility graphs," Phys. Rev. E **82**, 036120 (2010).
[31]B. Luque, L. Lacasa, J. F. Ballesteros, and R. Alberto, "Analytical properties of horizontal visibility graphs in the Feigenbaum scenario," Chaos **22**, 013109 (2012).
[32]B. Luque, L. Lacasa, and R. Alberto, "Feigenbaum graphs at the onset of chaos," Phys. Lett. A **376**, 3625–3629 (2012).
[33]M. McCullough, M. Small, T. Stemler, and H.-C. Iu, "Time lagged ordinal partition networks for capturing dynamics of continuous dynamical systems," Chaos **25**, 053101 (2015).
[34]M. Stephen, C.-G. Gu, and H.-J. Yang, "Visibility graph based time series analysis," PLoS One **10**(11), e0143015 (2015).
[35]A. Mary and Y. Lai, "Route to high-dimensional chaos," Phys. Rev. E **59**(4), R3799 (1999).
[36]M. Henon, "A two-dimensional mapping with a strange attractor," Commun. Math. Phys. **50**(1), 69–77 (1976).
[37]E. Lorenz, "Deterministic nonperiodic flow," J. Atmos. Sci. **20**(2), 130–141 (1963).
[38]J. Dormand and P. J. Prince, "A family of embedded Runge-Kutta formulae," J. Comput. Appl. Math. **6**, 19–26 (1980).
[39]L. Cao, "Practical method for determining the minimum embedding dimension of a scalar time series," Physica D **110**, 43–50 (1997).
[40]S. Strogatz, *Nonlinear Dynamics and Chaos: With Applications to Physics, Biology and Chemistry* (Perseus Publishing, 2001).
[41]R. May, "Simple mathematical models with very complicated dynamics," Nature **261**(5560), 459–467 (1976); M. J. Feigenbaum, "Quantitative Universality for a Class of Non-Linear Transformations," J. Stat. Phys. **19**(1), 25–52 (1978).
[42]S. Partha and S.-H. Strogatz, "The birth of period three," Math. Mag. **68**, 42–47 (1995).
[43]B. John, "The birth of period 3 revisited," Math. Mag. **69**(2), 115–118 (1996).
[44]J. F. Antonio and C. M. Luciano, "Algebraic orbits on period-3 window for the logistic map," Nonlinear Dyn. **79**(2), 1015–1021 (2015).
[45]C. Zhang, "Period three begins," Math. Mag. **83**, 295–297 (2010).
[46]A. Barrat, M. Barthelemy, and R. Pastor-Satorra, "The architecture of complex weighted networks," Proc. Natl. Acad. Sci. U.S.A. **101**(11), 3747–3752 (2004).
[47]R. Milo, S. Shen-Orr, S. Itzkovitz, N. Kashtan, D. Chklovskii, and U. Alon, "Network motifs: Simple building blocks of complex networks," Science **298**(5594), 824–827 (2002).
[48]A. Reka and A. Barabasi, "Statistical mechanics of complex networks," Rev. Mod. Phys. **74**(51), 47–97 (2002).
[49]J. Kantelhardt, S. Zschiegner, E. Koscielny, S. Havlin, A. Bunde, and E. Stanley, "Multifractal detrended fluctuation analysis of nonstationary time series," Physica A **316**, 87–114 (2002).
[50]L. Kristoufek, "Rescaled range analysis and detrended fluctuation analysis: Finite sample properties and confidence levels," AUCO Czech Econ. Rev. **4**(3), 315–329 (2010).
[51]C. Sparrow, *The Lorenz Equations: Bifurcations, Chaos, and Strange Attractors*, Applied Mathematical Sciences Vol. 41 (Springer-Verlag, Berlin, 1982), ISBN: 3-540-90775-0.